

Neutrino Interferometry for High-Precision Tests of Lorentz Symmetry with IceCube

M. G. Aartsen,¹ M. Ackermann,² J. Adams,³ J. A. Aguilar,⁴ M. Ahlers,⁵ M. Ahrens,⁶ I. Al Samarai,⁷ D. Altmann,⁸ K. Andeen,⁹ T. Anderson,¹⁰ I. Anseau,⁴ G. Anton,⁸ C. Argüelles,¹¹ J. Auffenberg,¹² S. Axani,¹¹ H. Bagherpour,³ X. Bai,¹³ J. P. Barron,¹⁴ S. W. Barwick,¹⁵ V. Baum,¹⁶ R. Bay,¹⁷ J. J. Beatty,^{18,19} J. Becker Tjus,²⁰ K.-H. Becker,²¹ S. BenZvi,²² D. Berley,²³ E. Bernardini,² D. Z. Besson,²⁴ G. Binder,^{25,17} D. Bindig,²¹ E. Blaufuss,²³ S. Blot,² C. Boehm,⁶ M. Börner,²⁶ F. Bos,²⁰ D. Bose,²⁷ S. Böser,¹⁶ O. Botner,²⁸ E. Bourbeau,⁵ J. Bourbeau,²⁹ F. Bradascio,² J. Braun,²⁹ L. Brayeur,³⁰ M. Brenzke,¹² H.-P. Bretz,² S. Bron,⁷ J. Brostean-Kaiser,² A. Burgman,²⁸ T. Carver,⁷ J. Casey,²⁹ M. Casier,³⁰ E. Cheung,²³ D. Chirkin,²⁹ A. Christov,⁷ K. Clark,³¹ L. Classen,³² S. Coenders,³³ G. H. Collin,¹¹ J. M. Conrad,¹¹ D. F. Cowen,^{10,34} R. Cross,²² M. Day,²⁹ J. P. A. M. de André,³⁵ C. De Clercq,³⁰ J. J. DeLaunay,¹⁰ H. Dembinski,³⁶ S. De Ridder,³⁷ P. Desiati,²⁹ K. D. de Vries,³⁰ G. de Wasseige,³⁰ M. de With,³⁸ T. DeYoung,³⁵ J. C. Díaz-Vélez,²⁹ V. di Lorenzo,¹⁶ H. Dujmovic,²⁷ J. P. Dumm,⁶ M. Dunkman,¹⁰ E. Dvorak,¹³ B. Eberhardt,¹⁶ T. Ehrhardt,¹⁶ B. Eichmann,²⁰ P. Eller,¹⁰ P. A. Evenson,³⁶ S. Fahey,²⁹ A. R. Fazely,³⁹ J. Felde,²³ K. Filimonov,¹⁷ C. Finley,⁶ S. Flis,⁶ A. Franckowiak,² E. Friedman,²³ T. Fuchs,²⁶ T. K. Gaisser,³⁶ J. Gallagher,⁴⁰ L. Gerhardt,²⁵ K. Ghorbani,²⁹ W. Giang,¹⁴ T. Glauch,¹² T. Glüsenkamp,⁸ A. Goldschmidt,²⁵ J. G. Gonzalez,³⁶ D. Grant,¹⁴ Z. Griffith,²⁹ C. Haack,¹² A. Hallgren,²⁸ F. Halzen,²⁹ K. Hanson,²⁹ D. Hebecker,³⁸ D. Heereman,⁴ K. Helbing,²¹ R. Hellauer,²³ S. Hickford,²¹ J. Hignight,³⁵ G. C. Hill,¹ K. D. Hoffman,²³ R. Hoffmann,²¹ B. Hokanson-Fasig,²⁹ K. Hoshina,^{29,41} F. Huang,¹⁰ M. Huber,³³ K. Hultqvist,⁶ M. Hünnefeld,²⁶ S. In,²⁷ A. Ishihara,⁴² E. Jacobi,² G. S. Japaridze,⁴³ M. Jeong,²⁷ K. Jero,²⁹ B. J. P. Jones,⁴⁴ P. Kalaczynski,¹² W. Kang,²⁷ A. Kappes,³² T. Karg,² A. Karle,²⁹ T. Katori,⁴⁵ U. Katz,⁸ M. Kauer,²⁹ A. Keivani,¹⁰ J. L. Kelley,²⁹ A. Kheirandish,²⁹ J. Kim,²⁷ M. Kim,⁴² T. Kintscher,² J. Kiryluk,⁴⁶ T. Kittler,⁸ S. R. Klein,^{25,17} G. Kohnen,⁴⁷ R. Koirala,³⁶ H. Kolanoski,³⁸ L. Köpke,¹⁶ C. Kopper,¹⁴ S. Kopper,⁴⁸ J. P. Koschinsky,¹² D. J. Koskinen,⁵ M. Kowalski,^{38,2} K. Krings,³³ M. Kroll,²⁰ G. Krückl,¹⁶ J. Kunnen,³⁰ S. Kunwar,² N. Kurahashi,⁴⁹ T. Kuwabara,⁴² A. Kyriacou,¹ M. Labare,³⁷ J. L. Lanfranchi,¹⁰ M. J. Larson,⁵ F. Lauber,²¹ M. Lesiak-Bzdak,⁴⁶ M. Leuermann,¹² Q. R. Liu,²⁹ L. Lu,⁴² J. Lünemann,³⁰ W. Luszczak,²⁹ J. Madsen,⁵⁰ G. Maggi,³⁰ K. B. M. Mahn,³⁵ S. Mancina,²⁹ S. Mandalia,⁴⁵ R. Maruyama,⁵¹ K. Mase,⁴² R. Maunu,²³ F. McNally,²⁹ K. Meagher,⁴ M. Medici,⁵ M. Meier,²⁶ T. Menne,²⁶ G. Merino,²⁹ T. Meures,⁴ S. Miarecki,^{25,17} J. Micallef,³⁵ G. Momenté,¹⁶ T. Montaruli,⁷ R. W. Moore,¹⁴ M. Moulai,¹¹ R. Nahnauer,² P. Nakarmi,⁴⁸ U. Naumann,²¹ G. Neer,³⁵ H. Niederhausen,⁴⁶ S. C. Nowicki,¹⁴ D. R. Nygren,²⁵ A. Obertacke Pollmann,²¹ A. Olivas,²³ A. O'Murchadha,⁴ T. Palczewski,^{25,17} H. Pandya,³⁶ D. V. Pankova,¹⁰ P. Peiffer,¹⁶ J. A. Pepper,⁴⁸ C. Pérez de los Heros,²⁸ D. Pieloth,²⁶ E. Pinat,⁴ M. Plum,⁹ P. B. Price,¹⁷ G. T. Przybylski,²⁵ C. Raab,⁴ L. Rädcl,¹² M. Rameez,⁵ K. Rawlins,⁵² I. C. Rea,³³ R. Reimann,¹² B. Relethford,⁴⁹ M. Relich,⁴² E. Resconi,³³ W. Rhode,²⁶ M. Richman,⁴⁹ S. Robertson,¹ M. Rongen,¹² C. Rott,²⁷ T. Ruhe,²⁶ D. Ryckbosch,³⁷ D. Rysewyk,³⁵ T. Sälzer,¹² S. E. Sanchez Herrera,¹⁴ A. Sandrock,²⁶ J. Sandroos,¹⁶ M. Santander,⁴⁸ S. Sarkar,^{5,53} S. Sarkar,¹⁴ K. Satalecka,² P. Schlunder,²⁶ T. Schmidt,²³ A. Schneider,²⁹ S. Schoenen,¹² S. Schöneberg,²⁰ L. Schumacher,¹² D. Seckel,³⁶ S. Seunarine,⁵⁰ J. Soedingrekso,²⁶ D. Soldin,²¹ M. Song,²³ G. M. Spiczak,⁵⁰ C. Spiering,² J. Stachurska,² M. Stamatikos,¹⁸ T. Stanev,³⁶ A. Stasik,² J. Stettner,¹² A. Steuer,¹⁶ T. Stezelberger,²⁵ R. G. Stokstad,²⁵ A. Stöbl,⁴² N. L. Strotjohann,² T. Stuttard,⁵ G. W. Sullivan,²³ M. Sutherland,¹⁸ I. Taboada,⁵⁴ J. Tatar,^{25,17} F. Tenholt,²⁰ S. Ter-Antonyan,³⁹ A. Terliuk,² G. Tešić,¹⁰ S. Tilav,³⁶ P. A. Toale,⁴⁸ M. N. Tobin,²⁹ S. Toscano,³⁰ D. Tosi,²⁹ M. Tselengidou,⁸ C. F. Tung,⁵⁴ A. Turcati,³³ C. F. Turley,¹⁰ B. Ty,²⁹ E. Unger,²⁸ M. Usner,² J. Vandenbroucke,²⁹ W. Van Driessche,³⁷ N. van Eijndhoven,³⁰ S. Vanheule,³⁷ J. van Santen,² M. Vehring,¹² E. Vogel,¹² M. Vraeghe,³⁷ C. Walck,⁶ A. Wallace,¹ M. Wallraff,¹² F. D. Wandler,¹⁴ N. Wandkowsky,²⁹ A. Waza,¹² C. Weaver,¹⁴ M. J. Weiss,¹⁰ C. Wendt,²⁹ J. Werthebach,²⁶ S. Westerhoff,²⁹ B. J. Whelan,¹ K. Wiebe,¹⁶ C. H. Wiebusch,¹² L. Wille,²⁹ D. R. Williams,⁴⁸ L. Wills,⁴⁹ M. Wolf,²⁹ J. Wood,²⁹ T. R. Wood,¹⁴ E. Woolsey,¹⁴ K. Woschnagg,¹⁷ D. L. Xu,²⁹ X. W. Xu,³⁹ Y. Xu,⁴⁶ J. P. Yanez,¹⁴ G. Yodh,¹⁵ S. Yoshida,⁴² T. Yuan,²⁹ and M. Zoll⁶

(IceCube Collaboration)*

¹Department of Physics, University of Adelaide, Adelaide, 5005, Australia

²DESY, D-15738 Zeuthen, Germany

³Dept. of Physics and Astronomy, University of Canterbury, Private Bag 4800, Christchurch, New Zealand

⁴Université Libre de Bruxelles, Science Faculty CP230, B-1050 Brussels, Belgium

⁵Niels Bohr Institute, University of Copenhagen, DK-2100 Copenhagen, Denmark

⁶Oskar Klein Centre and Dept. of Physics, Stockholm University, SE-10691 Stockholm, Sweden

⁷Département de physique nucléaire et corpusculaire,

Université de Genève, CH-1211 Genève, Switzerland

- ⁸*Erlangen Centre for Astroparticle Physics, Friedrich-Alexander-Universität Erlangen-Nürnberg, D-91058 Erlangen, Germany*
- ⁹*Department of Physics, Marquette University, Milwaukee, WI, 53201, USA*
- ¹⁰*Dept. of Physics, Pennsylvania State University, University Park, PA 16802, USA*
- ¹¹*Dept. of Physics, Massachusetts Institute of Technology, Cambridge, MA 02139, USA*
- ¹²*III. Physikalisches Institut, RWTH Aachen University, D-52056 Aachen, Germany*
- ¹³*Physics Department, South Dakota School of Mines and Technology, Rapid City, SD 57701, USA*
- ¹⁴*Dept. of Physics, University of Alberta, Edmonton, Alberta, Canada T6G 2E1*
- ¹⁵*Dept. of Physics and Astronomy, University of California, Irvine, CA 92697, USA*
- ¹⁶*Institute of Physics, University of Mainz, Staudinger Weg 7, D-55099 Mainz, Germany*
- ¹⁷*Dept. of Physics, University of California, Berkeley, CA 94720, USA*
- ¹⁸*Dept. of Physics and Center for Cosmology and Astro-Particle Physics, Ohio State University, Columbus, OH 43210, USA*
- ¹⁹*Dept. of Astronomy, Ohio State University, Columbus, OH 43210, USA*
- ²⁰*Fakultät für Physik & Astronomie, Ruhr-Universität Bochum, D-44780 Bochum, Germany*
- ²¹*Dept. of Physics, University of Wuppertal, D-42119 Wuppertal, Germany*
- ²²*Dept. of Physics and Astronomy, University of Rochester, Rochester, NY 14627, USA*
- ²³*Dept. of Physics, University of Maryland, College Park, MD 20742, USA*
- ²⁴*Dept. of Physics and Astronomy, University of Kansas, Lawrence, KS 66045, USA*
- ²⁵*Lawrence Berkeley National Laboratory, Berkeley, CA 94720, USA*
- ²⁶*Dept. of Physics, TU Dortmund University, D-44221 Dortmund, Germany*
- ²⁷*Dept. of Physics, Sungkyunkwan University, Suwon 440-746, Korea*
- ²⁸*Dept. of Physics and Astronomy, Uppsala University, Box 516, S-75120 Uppsala, Sweden*
- ²⁹*Dept. of Physics and Wisconsin IceCube Particle Astrophysics Center, University of Wisconsin, Madison, WI 53706, USA*
- ³⁰*Vrije Universiteit Brussel (VUB), Dienst ELEM, B-1050 Brussels, Belgium*
- ³¹*SNOLAB, 1039 Regional Road 24, Creighton Mine 9, Lively, ON, Canada P3Y 1N2*
- ³²*Institut für Kernphysik, Westfälische Wilhelms-Universität Münster, D-48149 Münster, Germany*
- ³³*Physik-department, Technische Universität München, D-85748 Garching, Germany*
- ³⁴*Dept. of Astronomy and Astrophysics, Pennsylvania State University, University Park, PA 16802, USA*
- ³⁵*Dept. of Physics and Astronomy, Michigan State University, East Lansing, MI 48824, USA*
- ³⁶*Bartol Research Institute and Dept. of Physics and Astronomy, University of Delaware, Newark, DE 19716, USA*
- ³⁷*Dept. of Physics and Astronomy, University of Gent, B-9000 Gent, Belgium*
- ³⁸*Institut für Physik, Humboldt-Universität zu Berlin, D-12489 Berlin, Germany*
- ³⁹*Dept. of Physics, Southern University, Baton Rouge, LA 70813, USA*
- ⁴⁰*Dept. of Astronomy, University of Wisconsin, Madison, WI 53706, USA*
- ⁴¹*Earthquake Research Institute, University of Tokyo, Bunkyo, Tokyo 113-0032, Japan*
- ⁴²*Dept. of Physics and Institute for Global Prominent Research, Chiba University, Chiba 263-8522, Japan*
- ⁴³*CTSPS, Clark-Atlanta University, Atlanta, GA 30314, USA*
- ⁴⁴*Dept. of Physics, University of Texas at Arlington, 502 Yates St., Science Hall Rm 108, Box 19059, Arlington, TX 76019, USA*
- ⁴⁵*School of Physics and Astronomy, Queen Mary University of London, London E1 4NS, UK*
- ⁴⁶*Dept. of Physics and Astronomy, Stony Brook University, Stony Brook, NY 11794-3800, USA*
- ⁴⁷*Université de Mons, 7000 Mons, Belgium*
- ⁴⁸*Dept. of Physics and Astronomy, University of Alabama, Tuscaloosa, AL 35487, USA*
- ⁴⁹*Dept. of Physics, Drexel University, 3141 Chestnut Street, Philadelphia, PA 19104, USA*
- ⁵⁰*Dept. of Physics, University of Wisconsin, River Falls, WI 54022, USA*
- ⁵¹*Dept. of Physics, Yale University, New Haven, CT 06520, USA*
- ⁵²*Dept. of Physics and Astronomy, University of Alaska Anchorage, 3211 Providence Dr., Anchorage, AK 99508, USA*
- ⁵³*Dept. of Physics, University of Oxford, 1 Keble Road, Oxford OX1 3NP, UK*
- ⁵⁴*School of Physics and Center for Relativistic Astrophysics, Georgia Institute of Technology, Atlanta, GA 30332, USA*

Lorentz symmetry is a fundamental space-time symmetry underlying both the Standard Model of particle physics and general relativity. This symmetry guarantees that physical phenomena are observed to be the same by all inertial observers. However, unified theories, such as string theory, allow for violation of this symmetry by inducing new space-time structure at the quantum gravity scale. Thus, the discovery of Lorentz symmetry violation could be the first hint of these theories in Nature. Here we report the results of the most precise test of space-time symmetry in the neutrino sector to date. We use high-energy atmospheric neutrinos observed at the IceCube Neutrino Observatory to search for anomalous neutrino oscillations as signals of Lorentz violation. We find no evidence for such phenomena. This allows us to constrain the size of the dimension-four

operator in the Standard-Model Extension for Lorentz violation to the 10^{-28} level and to set limits on higher dimensional operators in this framework. These are among the most stringent limits on Lorentz violation set by any physical experiment.

INTRODUCTION

Very small violations of Lorentz symmetry, or “Lorentz violation” (LV), are allowed in many ultra-high-energy theories, including string theory [1], noncommutative field theory [2], and supersymmetry [3]. The discovery of LV could be the first indication of such new physics. Because of this, there are world-wide efforts underway to search for evidence of LV. The Standard-Model Extension (SME) is an effective-field-theory framework to systematically study LV [4]. The SME includes all possible types of LV which respect other symmetries of the Standard Model such as energy-momentum conservation and coordinate independence. Thus, the SME can provide a framework to compare results of LV searches from many different fields such as photons [5–8], nucleons [9–11], charged leptons [12–14], and gravity [15]. Recently, neutrino experiments have performed searches for LV [16–18]. So far all searches have obtained null results. The full list of existing limits from all sectors and a brief overview of the field are available elsewhere [19, 20]. Our focus here is to present the most precise test of LV in the neutrino sector.

The fact that neutrinos have mass has been established by a series of experiments [21–26]. The field has incorporated these results into the “neutrino Standard Model” (ν SM)—the SM with three massive neutrinos. Although the ν SM parameters are not yet fully determined [27], the model is rigorous enough to be brought to bear on the question of LV. We briefly review in Methods the history of neutrino oscillation physics and tests of Lorentz violation with neutrinos.

To date, neutrino masses have proved to be too small to be measured kinematically, but the mass differences are known via neutrino oscillations. This phenomenon arises from the fact that production and detection of neutrinos involves the flavour states, while the propagation is given by the Hamiltonian eigenstates. Thus, a neutrino with flavour $|\nu_\alpha\rangle$ can be written as a superposition of Hamiltonian eigenstates $|\nu_i\rangle$, i.e., $|\nu_\alpha\rangle = \sum_{i=1}^3 V_{\alpha i}(E)|\nu_i\rangle$, where V is the unitary matrix that diagonalizes the Hamiltonian and in general is a function of neutrino energy E . When the neutrino travels in vacuum without new physics, the Hamiltonian depends only on the neutrino masses, and the Hamiltonian eigenstates coincide with the mass eigenstates. That is, $H = \frac{1}{2E} \cdot U^\dagger \text{diag}(m_1^2, m_2^2, m_3^2)U = \frac{m^2}{2E}$, where m_i are the neutrino masses and U is the PMNS matrix which diagonalizes the mass matrix m [27].

A consequence of the flavour misalignment is that a neutrino beam that is produced purely of one flavour

will evolve to produce other flavours. Experiments measure the number of neutrinos of different flavours, observed as a function of the reconstructed energy of the neutrino, E , and the distance the beam has traveled, L . The microscopic neutrino masses are directly tied to the macroscopic neutrino oscillation length. In this sense, neutrino oscillations are similar to photon interference experiments in their ability to probe very small scales in Nature.

LORENTZ VIOLATING NEUTRINO OSCILLATIONS

In this analysis, we use neutrino oscillations as a natural interferometer with a size equal to the diameter of the Earth. We look for anomalous flavour-changing effects caused by LV that would modify the observed energy and zenith angle distributions of atmospheric muon neutrinos observed in the IceCube Neutrino Observatory [28] (see Figure 1). Beyond flavour change due to small neutrino masses, any hypothetical LV fields could contribute to muon neutrino flavour conversion. Thus, in this analysis, we look for distortion of the expected muon neutrino distribution. Since this analysis does not distinguish between a muon neutrino (ν_μ) and its antineutrino ($\bar{\nu}_\mu$), when the word “neutrino” is used, we are referring to both.

Past searches for LV have mainly focused on the directional effect in the Sun-centred celestial-equatorial frame (SCCEF) [19] by looking only at the time dependence of physics observables as direction-dependent physics appears as a function of the Earth’s rotation. However, in our case, we assume no time dependence, and instead look at the energy distribution distortions caused by direction- and time-independent isotropic LV. Isotropic LV may be a factor $\sim 10^3$ larger than direction-dependent LV in SCCEF if we assume that the new physics is isotropic in the CMB frame [20]. It would be most optimal to simultaneously look for both effects, but our limited statistics do not allow for this.

To calculate the effect, we start from an effective Hamiltonian derived from the SME [4], which can be written as

$$H \sim \frac{m^2}{2E} + \mathring{a}^{(3)} - E \cdot \mathring{c}^{(4)} + E^2 \cdot \mathring{a}^{(5)} - E^3 \cdot \mathring{c}^{(6)} \dots \quad (1)$$

The first term of Eq. (1) is from the ν SM, however, its impact decreases at high energy. The remaining terms ($\mathring{a}^{(3)}$, $\mathring{c}^{(4)}$, $\mathring{a}^{(5)}$, and so on) arise from the SME and describe isotropic Lorentz violating effects. The circle symbol on top indicates isotropic coefficients, and the

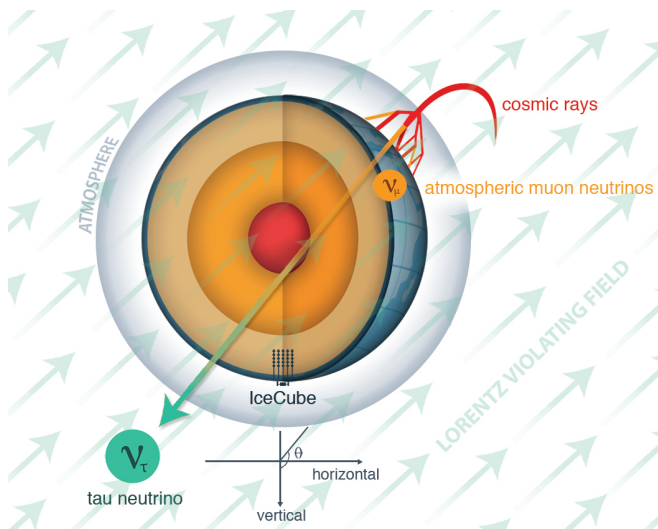


FIG. 1: Schematic figure of the test of LV with atmospheric neutrinos in IceCube. Muon neutrinos produced in the upper atmosphere are detected by IceCube in Antarctica. The potential signal is the anomalous disappearance of muon neutrinos, which might be caused by the presence of a hypothetical LV field that permeates space. The effect can be directional (arrows), but in this analysis we test the isotropic component.

number in the bracket is the dimension of the operator. These terms are typically classified as CPT-odd ($\hat{a}^{(d)}$) and CPT-even ($\hat{c}^{(d)}$). Focusing on muon neutrino to tau neutrino ($\nu_\mu \rightarrow \nu_\tau$) oscillations, all SME terms in Eq. (1) can be expressed as 2×2 matrices, such as

$$\hat{c}^{(6)} = \begin{pmatrix} \hat{c}_{\mu\mu}^{(6)} & \hat{c}_{\mu\tau}^{(6)} \\ \hat{c}_{\mu\tau}^{(6)*} & -\hat{c}_{\mu\mu}^{(6)} \end{pmatrix}. \quad (2)$$

Without loss of generality, we can define the matrices so that they are traceless, leaving three independent parameters, in this case: $\hat{c}_{\mu\mu}^{(6)}$, $\text{Re}(\hat{c}_{\mu\tau}^{(6)})$, and $\text{Im}(\hat{c}_{\mu\tau}^{(6)})$. The off-diagonal Lorentz violating term $\hat{c}_{\mu\tau}^{(6)}$ dominates neutrino oscillations at high energy, which is the main interest of this paper. In this formalism, LV can be described by an infinite series, but higher order terms are expected to be suppressed. Therefore, most terrestrial experiments focus on searching for effects of dimension-three and -four operators; $\hat{a}^{(3)}$ and $E \cdot \hat{c}^{(4)}$ respectively. However, our analysis extends to dimension-eight, *i.e.*, $E^2 \cdot \hat{a}^{(5)}$, $E^3 \cdot \hat{c}^{(6)}$, $E^4 \cdot \hat{a}^{(7)}$, and $E^5 \cdot \hat{c}^{(8)}$. Such higher orders are accessible by IceCube, which observes high-energy neutrinos where we expect an enhancement from the terms with dimension greater than four. In fact, some theories, such as noncommutative field theory [2] and supersymmetry [3], allow for LV to appear in higher order operators. As an example, we expect dimension-six new physics operators of order $\sim \frac{1}{M_P^2} \sim 10^{-38} \text{ GeV}^{-2}$ where M_P is the Planck mass which is the natural energy scale of the unification of all matter and forces including gravity. We assume

that only one dimension is important at any given energy scale, because the strength of LV is expected to be different at different orders.

We use the $\nu_\mu \rightarrow \nu_\tau$ two-flavour oscillation scheme following Ref. [29]. This is appropriate because we assume there is no significant interference with ν_e . Details of the model used in this analysis are given in Methods. The oscillation probability is given by

$$P(\nu_\mu \rightarrow \nu_\tau) = -4V_{\mu 1}V_{\mu 2}V_{\tau 1}V_{\tau 2} \sin^2 \left(\frac{\lambda_2 - \lambda_1}{2} L \right), \quad (3)$$

where $V_{\alpha i}$ are the mixing matrix elements of the effective Hamiltonian (Eq. (1)), and λ_i are its eigenvalues. Both mixing matrix elements and eigenvalues are a function of energy, ν SM oscillation parameters, and SME coefficients. Full expressions are given in Supplementary material Appendix A.

THE ICECUBE NEUTRINO OBSERVATORY

The IceCube Neutrino Observatory is located at the geographic South Pole [30, 31]. The detector volume is one cubic kilometer of clear Antarctic ice. Atmospheric muon neutrinos interacting on surrounding ice or bedrock may produce high-energy muons, which emit photons that are subsequently detected by digital optical modules (DOMs) embedded in the ice. The DOMs consist of a 25 cm diameter Hamamatsu photomultiplier tube, with readout electronics, contained within a 36.5 cm glass pressure housing. These are installed in holes in the ice with roughly 125 m separation. There are 86 holes in the ice with a total of 5160 DOMs, which are distributed at depths of 1450 m to 2450 m below the surface, instrumenting one gigaton of ice. The full detector description can be found in Ref. [31].

This detector observes Cherenkov light from muons produced in charged-current ν_μ interactions. Photons detected by the DOMs allow for the reconstruction of the muon energy and direction, which is related to the energy of the primary ν_μ . Because the muons are above critical energy, their energy can be determined by measuring the stochastic losses that produce Cherenkov light. See Ref. [28] for details on the muon energy proxy used in this analysis. In the TeV energy range, these muons traverse distances of order kilometers, and have small scattering angle due to the large Lorentz boost, resulting in 0.75° resolution on the reconstructed direction at 1 TeV [32]. We use up-going muon data of TeV-scale energy from two years of detector operation [28] representing 34975 events with a 0.1% atmospheric muon contamination.

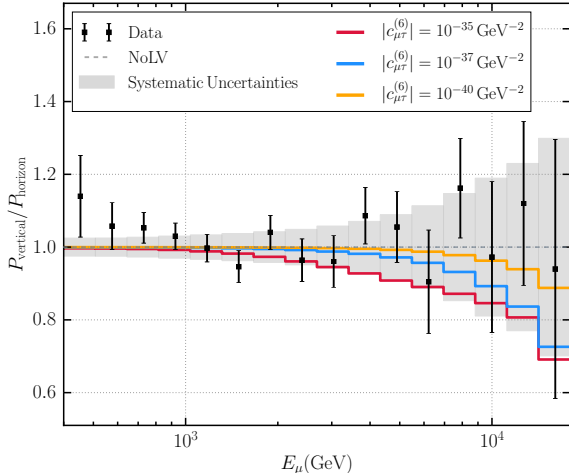


FIG. 2: The ratio of vertical to horizontal neutrino transition probabilities at IceCube. Here, vertical events are defined by $\cos\theta \leq -0.6$ and the horizontal events are defined by $\cos\theta > -0.6$. The transition probability ratio with one standard deviation statistical errors, are extracted from the data, is compared to the prediction for various dimension-six operator values: $10^{-35} \text{ GeV}^{-2}$ (red), $10^{-37} \text{ GeV}^{-2}$ (blue), and $10^{-40} \text{ GeV}^{-2}$ (yellow). The range of uncorrelated systematic uncertainties is shown as a light grey band. This is constructed from ensembles of many simulations where the nuisance parameters are varied within their uncertainties.

ANALYSIS SETUP

To obtain the prediction for LV effects, we multiply the oscillation probability, given in Eq. (3), with the predicted atmospheric neutrino flux calculated using the matrix cascade equation (MCEq) [33]. These “atmospheric neutrinos” originate from decays of muons and various mesons produced by collisions of primary cosmic rays and air molecules, and consist of both neutrinos and antineutrinos. The atmospheric neutrinos have two main components: “conventional,” from pion and kaon decay, and “prompt,” from charmed meson decay. The conventional flux dominates at energies less than 18 TeV because of the larger production cross section, whereas the harder prompt spectrum becomes relevant at higher energy. In the energy range of interest, the astrophysical neutrino contribution is small. We include it modelled as a power law with normalization and spectral index, $\sim \Phi \cdot E^{-\gamma}$. The absorption of each flux component propagating through the Earth to IceCube is properly modelled [34, 35]. Muon production from ν_μ charged-current events at IceCube proceeds through deep inelastic neutrino interactions as calculated in Ref. [36].

The short distance of travel for horizontal neutrinos leads to negligible spectral distortion due to LV, while the long pathlength for vertical neutrinos leads to modi-

fications. Therefore, if we compare the zenith angle distribution (θ) of the expectation from simulations and ν_μ data from $\cos\theta = -1.0$ (vertical) to $\cos\theta = 0.0$ (horizontal), see Fig. 1, then one can determine the allowed LV parameters. Figure 2 shows the ratio of transition probabilities of vertical events to horizontal events. The data transition probability is defined by the ratio of observed events to expected events, and the simulation transition probability is defined by the expected events in the presence of LV to the number of events in the absence of LV. In the absence of LV, this ratio equals one. Here, as an example, we show several predictions from simulations with different dimension-six LV parameters $|c_{\mu\tau}^{(6)}|$. In general, higher order terms are more important at higher energies. In order to assess the existence of LV, we perform a binned Poisson likelihood analysis by binning the data in zenith angle and energy. We use 10 linearly-spaced bins in cosine of zenith angle from -1.0 to 0.0 and 17 logarithmically-spaced bins in reconstructed muon energy ranging from 400 GeV to 18 TeV. Systematic uncertainties are incorporated as nuisance parameters in our likelihood. We introduce six systematic parameters related to the neutrino flux prediction: normalizations of conventional (40% error), prompt (no constraint), and astrophysical (no constraint) neutrino flux components; ratio of pion and kaon contributions for conventional flux (10% error); spectral index of primary cosmic rays (2% error); and astrophysical neutrino spectral index (25% error). The absolute photon detection efficiency has been shown to have negligible impact on the exclusion contours in a search for sterile neutrinos that uses an equivalent analysis technique for a subset of the IceCube data considered here [34, 37]. The impact of light propagation model uncertainties on the horizontal to vertical ratio is less than 5% at few TeV, where this analysis is most sensitive [35]. Thus the impact of these uncertainties on the exclusion contours are negligible.

To constrain the LV parameters we use two statistical techniques. First, we performed a likelihood analysis by profiling the likelihood over the nuisance parameters per set of LV parameters. From the profiled likelihood, we find the best-fit LV parameters and derive the 90% and 99% confidence levels (C.L.) assuming Wilks’ theorem with three degrees of freedom [37]. Second, we set the priors to the nuisance parameter uncertainties and scan the posterior space of the likelihood by means of a Markov Chain Monte Carlo (MCMC) method [38]. These two procedures are found to be complementary, and the extracted LV parameters agree with the null hypothesis. For simplicity, we present the likelihood results in this paper and show the MCMC results in Methods Supplementary material Appendix B.

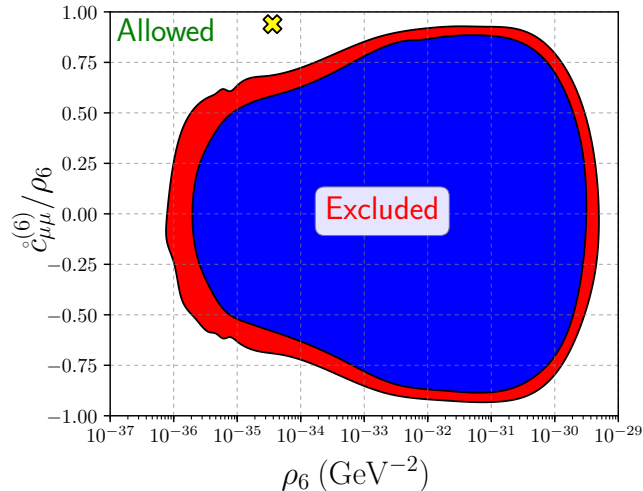


FIG. 3: The excluded parameter space region for the dimension-six SME coefficients. The parameters of horizontal and vertical axes are combinations of the three SME coefficients and explained in text. The best-fit point is shown by the yellow cross and the blue (red) region is excluded at 99% (90%) C.L.

RESULTS

Figure 3 shows the excluded region of dimension-six SME coefficients. The results for all operators are available in Supplementary material Appendix C. The fit was performed in a three-dimensional phase space; however, the complex phase of the off-diagonal terms is not important at high energy, and we choose the following representation methods. The horizontal axis shows the strength of LV, $\rho_6 \equiv \sqrt{(\hat{c}_{\mu\mu}^{(6)})^2 + \text{Re}(\hat{c}_{\mu\tau}^{(6)})^2 + \text{Im}(\hat{c}_{\mu\tau}^{(6)})^2}$, and the vertical axis represents a fraction of the diagonal element, $\hat{c}_{\mu\mu}^{(6)}/\rho_6$. The best-fit point shown by the marker is compatible with the absence of LV; therefore, we present 90% C.L. (red) and 99% C.L. (blue) exclusion regions. The contour extends to small values, beyond the phase space explored by previous analyses [16–18]. The leftmost edge of our exclusion region is limited by the small statistics of high-energy atmospheric neutrinos. The rightmost edge of the exclusion region is limited by fast LV-induced oscillations that suppress the flux but lead to no shape distortion. This can only be constrained by the absolute normalization of the flux. In the case of the dimension-three operator, the right edge can be excluded by other atmospheric neutrino oscillation measurements [18, 39]. We have studied the applicability of Wilks’ theorem via simulations. Near degenerate real and imaginary parameters reduce the expected degrees of freedom from three and the results here are interpreted as conservative confidence intervals.

Unlike previous results [16–18], this analysis includes all parameter correlations, allowing for certain combina-

tions of parameters to be unconstrained. This can be seen near $\hat{c}_{\mu\mu}^{(6)}/\rho_6 = -1$ and 1, where LV is dominated by the large diagonal component. This induces the quantum Zeno effect [40], where a neutrino flavour state is “arrested” in one state by a continuous interaction with a LV field suppressing flavour transitions. Thus, the unshaded regions below and above our exclusion zone are very difficult to constrain with terrestrial experiments.

Table I summarizes the results of this work along with representative best limits. A comprehensive list of LV tests is available in [19]. To date, there is no experimental indication of LV, and all these experiments have maximized their limits by assuming that all but one of the SME parameters are zero [19]. Therefore, to make our results comparable with previous limits, we adopt the same convention. For this, we set the diagonal SME parameters to zero and focus on setting limits on the off-diagonal elements. The details of the procedure used to set limits are given in Supplementary material Appendix D.

Let us consider the limits from the lowest to highest order. Dimension-three and -four operators are included in the renormalizable sector of SME. These are the main focus of experiments using photons [7, 8], nucleons [10, 11], and charged leptons [12–14]. Going beyond terrestrial experiments, limits arising from astrophysical observations provide strong constraints [5, 6]. Among the variety of limits coming from the neutrino sector, the attainable best limits are dominated by atmospheric neutrino oscillation analyses [16–18], where the longest propagation length and the highest energies enable us to use neutrino oscillations as the biggest interferometer on the Earth. The results from our analysis surpass past ones due to the higher statistics of high-energy atmospheric neutrinos and our improved control of systematic uncertainties. Using a traditional metric, which assumes neutrinos to be massless, we can recast our result as an upper limit on any deviation of the speed of massless neutrinos from the speed of light due to LV. That is less than 10^{-28} at 99% CL. This is about an order of magnitude improvement over past analyses [16–18], and is of the same order as the deviation in speed that is expected due to the known neutrino mass at the energies relevant for this analysis.

Searches of dimension-five and higher LV operators are dominated by astrophysical observations [6, 9, 15]. Among them, ultra-high-energy cosmic rays (UHECRs) have the highest measured energy [41] and are used to set the strongest limits on dimension-six and higher operators [9]. However, these limits are sensitive to the composition of UHECRs, which is currently uncertain [20, 42]. These limits assume that the cosmic rays at the highest energies are protons, but if they are in fact iron nuclei, then the UHECR limits are significantly reduced. Our analysis sets the most stringent limits in an unambiguous way across all fields for the dimension-six operator. Such high-dimension operators are generic signatures of new physics [43]. For example, dimension-five operator

dim.	method	type	sector	limits	ref.
3	CMB polarization	astrophysical	photon	$\sim 10^{-43}$ GeV	[5]
	He-Xe comagnetometer	tabletop	neutron	$\sim 10^{-34}$ GeV	[10]
	torsion pendulum	tabletop	electron	$\sim 10^{-31}$ GeV	[12]
	muon g-2	accelerator	muon	$\sim 10^{-24}$ GeV	[13]
	neutrino oscillation	atmospheric	neutrino	$ \text{Re}(\hat{a}_{\mu\tau}^{(3)}) , \text{Im}(\hat{a}_{\mu\tau}^{(3)}) < 2.9 \times 10^{-24}$ GeV (99% C.L.) $< 2.0 \times 10^{-24}$ GeV (90% C.L.)	this work
4	GRB vacuum birefringence	astrophysical	photon	$\sim 10^{-38}$	[6]
	Laser interferometer	LIGO	photon	$\sim 10^{-22}$	[7]
	Sapphire cavity oscillator	tabletop	photon	$\sim 10^{-18}$	[8]
	Ne-Rb-K comagnetometer	tabletop	neutron	$\sim 10^{-29}$	[11]
	trapped Ca^+ ion	tabletop	electron	$\sim 10^{-19}$	[14]
neutrino oscillation	atmospheric	neutrino	$ \text{Re}(\hat{c}_{\mu\tau}^{(4)}) , \text{Im}(\hat{c}_{\mu\tau}^{(4)}) < 3.9 \times 10^{-28}$ (99% C.L.) $< 2.7 \times 10^{-28}$ (90% C.L.)	this work	
5	GRB vacuum birefringence	astrophysical	photon	$\sim 10^{-34}$ GeV $^{-1}$	[6]
	ultra-high-energy cosmic ray	astrophysical	proton	$\sim 10^{-22}$ to 10^{-18} GeV $^{-1}$	[9]
	neutrino oscillation	atmospheric	neutrino	$ \text{Re}(\hat{a}_{\mu\tau}^{(5)}) , \text{Im}(\hat{a}_{\mu\tau}^{(5)}) < 2.3 \times 10^{-32}$ GeV $^{-1}$ (99% C.L.) $< 1.5 \times 10^{-32}$ GeV $^{-1}$ (90% C.L.)	this work
6	GRB vacuum birefringence	astrophysical	photon	$\sim 10^{-31}$ GeV $^{-2}$	[6]
	ultra-high-energy cosmic ray	astrophysical	proton	$\sim 10^{-42}$ to 10^{-35} GeV $^{-2}$	[9]
	gravitational Cherenkov radiation	astrophysical	gravity	$\sim 10^{-31}$ GeV $^{-2}$	[15]
	neutrino oscillation	atmospheric	neutrino	$ \text{Re}(\hat{c}_{\mu\tau}^{(6)}) , \text{Im}(\hat{c}_{\mu\tau}^{(6)}) < 1.5 \times 10^{-36}$ GeV $^{-2}$ (99% C.L.) $< 9.1 \times 10^{-37}$ GeV $^{-2}$ (90% C.L.)	this work
7	GRB vacuum birefringence	astrophysical	photon	$\sim 10^{-28}$ GeV $^{-3}$	[6]
	neutrino oscillation	atmospheric	neutrino	$ \text{Re}(\hat{a}_{\mu\tau}^{(7)}) , \text{Im}(\hat{a}_{\mu\tau}^{(7)}) < 8.3 \times 10^{-41}$ GeV $^{-3}$ (99% C.L.) $< 3.6 \times 10^{-41}$ GeV $^{-3}$ (90% C.L.)	this work
8	gravitational Cherenkov radiation	astrophysical	gravity	$\sim 10^{-46}$ GeV $^{-4}$	[15]
	neutrino oscillation	atmospheric	neutrino	$ \text{Re}(\hat{c}_{\mu\tau}^{(8)}) , \text{Im}(\hat{c}_{\mu\tau}^{(8)}) < 5.2 \times 10^{-45}$ GeV $^{-4}$ (99% C.L.) $< 1.4 \times 10^{-45}$ GeV $^{-4}$ (90% C.L.)	this work

TABLE I: Comparison of attainable best limits of SME coefficients in various fields.

is an attractive possibility to produce neutrino masses, and dimension-six operators represent new physics interactions which can, for example, mediate proton decay. Although LV dimension-six operators, such as $\hat{c}_{\mu\tau}^{(6)}$, are well motivated by certain theories including noncommutative field theory [2] and supersymmetry [3], they have so far not been probed with elementary particles due to the lack of available high-energy sources. Thus, our work pushes boundaries on new physics beyond the Standard Model and general relativity.

CONCLUSION

We have presented a test of Lorentz violation with high-energy atmospheric muon neutrinos from IceCube. Correlations of the SME coefficients are fully taken into account, and systematic errors are controlled by the fit. Although we did not find evidence for LV, this analysis provides the best attainable limits on SME coefficients in the neutrino sector along with limits on the higher order operators. Comparison with limits from other sectors reveals that this work provides among the best attainable limits on dimension-six coefficients across all fields: from tabletop experiments to cosmology. This is a remarkable point that demonstrates how powerful neutrino interfer-

ometry can be in the study of fundamental space-time properties.

Further improvements on the search for LV in the neutrino sector using IceCube will be possible when the astrophysical neutrino sample is included [44]. Such analyses [45, 46] will require a substantial improvement of detector and flux systematic uncertainty evaluations [47, 48]. In the near future, water-based neutrino telescopes such as KM3NeT [49] and the ten-times-larger IceCube-Gen2 [50] will be in a position to observe more astrophysical neutrinos. With the higher statistics and improved sensitivity, these experiments will have an enhanced potential for discovery of Lorentz violation.

Data availability

The data that were used in this study are available in the IceCube Public Data Access "Astrophysical muon neutrino flux in the northern sky with 2 years of IceCube data [28]" [hyperlink to <http://icecube.wisc.edu/science/data/>].

* Corresponding authors: C. Argüelles (caad@mit.edu), G. H. Collin (gabrielc@mit.edu), J. M. Conrad (conrad@mit.edu), T. Katori (t.katori@qmul.ac.uk), A. Kheirandish (akheirandish@icecube.wisc.edu), and S. Mandalia (s.p.mandalia@qmul.ac.uk).

References

- [1] V. A. Kostelecký and S. Samuel, “Spontaneous Breaking of Lorentz Symmetry in String Theory,” *Phys. Rev. D* **39**, 683-685 (1989).
- [2] S. M. Carroll, J. A. Harvey, V. A. Kostelecky, C. D. Lane and T. Okamoto, *Phys. Rev. Lett.* **87**, 141601 (2001).
- [3] S. Groot Nibbelink and M. Pospelov, “Lorentz violation in supersymmetric field theories,” *Phys. Rev. Lett.* **94**, 081601 (2005).
- [4] A. Kostelecký and M. Mewes, “Neutrinos with Lorentz-violating operators of arbitrary dimension,” *Phys. Rev. D* **85**, 096005 (2012).
- [5] E. Komatsu *et al.* [WMAP Collaboration], “Five-Year Wilkinson Microwave Anisotropy Probe (WMAP) Observations: Cosmological Interpretation,” *Astrophys. J. Suppl.* **180**, 330-376 (2009).
- [6] V. A. Kostelecký and M. Mewes, “Constraints on relativity violations from gamma-ray bursts,” *Phys. Rev. Lett.* **110**, no. 20, 201601 (2013).
- [7] V. A. Kostelecký, A. C. Melissinos and M. Mewes, “Searching for photon-sector Lorentz violation using gravitational-wave detectors,” *Phys. Lett. B* **761**, 1-7 (2016).
- [8] M. Nagel *et al.*, “Direct Terrestrial Test of Lorentz Symmetry in Electrodynamics to 10^{-18} ,” *Nature Commun.* **6**, 8174 (2015).
- [9] L. Maccione, A. M. Taylor, D. M. Mattingly and S. Liberati, “Planck-scale Lorentz violation constrained by Ultra-High-Energy Cosmic Rays,” *JCAP* **0904**, 022 (2009).
- [10] F. Allmendinger *et al.*, “New Limit on Lorentz-Invariance- and CPT-Violating Neutron Spin Interactions Using a Free-Spin-Precession $^3\text{He} - ^{129}\text{Xe}$ Comagnetometer,” *Phys. Rev. Lett.* **112**, no. 11, 110801 (2014).
- [11] M. Smiciklas, J. M. Brown, L. W. Cheuk and M. V. Romalis, “A new test of local Lorentz invariance using ^{21}Ne -Rb-K comagnetometer,” *Phys. Rev. Lett.* **107**, 171604 (2011).
- [12] B. R. Heckel *et al.*, “New CP-violation and preferred-frame tests with polarized electrons,” *Phys. Rev. Lett.* **97**, 021603 (2006).
- [13] G. W. Bennett *et al.* [Muon (g-2) Collaboration], “Search for Lorentz and CPT violation effects in muon spin precession,” *Phys. Rev. Lett.* **100**, 091602 (2008).
- [14] T. Pruttivarasin *et al.*, “A Michelson-Morley Test of Lorentz Symmetry for Electrons,” *Nature* **517**, 592-595 (2015).
- [15] V. A. Kostelecký and J. D. Tasson, “Constraints on Lorentz violation from gravitational Čerenkov radiation,” *Phys. Lett. B* **749**, 551-559 (2015).
- [16] R. Abbasi *et al.* [IceCube Collaboration], “Determination of the Atmospheric Neutrino Flux and Searches for New Physics with AMANDA-II,” *Phys. Rev. D* **79**, 102005 (2009).
- [17] R. Abbasi *et al.* [IceCube Collaboration], “Search for a Lorentz-violating sidereal signal with atmospheric neutrinos in IceCube,” *Phys. Rev. D* **82**, 112003 (2010).
- [18] K. Abe *et al.* [Super-Kamiokande Collaboration], “Test of Lorentz invariance with atmospheric neutrinos,” *Phys. Rev. D* **91**, no. 5, 052003 (2015).
- [19] V. A. Kostelecky and N. Russell, “Data Tables for Lorentz and CPT Violation,” *Rev. Mod. Phys.* **83**, 11-31 (2011).
- [20] S. Liberati, “Tests of Lorentz invariance: a 2013 update,” *Class. Quant. Grav.* **30**, 133001 (2013).
- [21] Y. Fukuda *et al.* [Super-Kamiokande Collaboration], “Evidence for oscillation of atmospheric neutrinos,” *Phys. Rev. Lett.* **81**, 1562-1567 (1998).
- [22] Q. R. Ahmad *et al.* [SNO Collaboration], “Measurement of the rate of $\nu_e + d \rightarrow p + p + e^-$ interactions produced by ^8B solar neutrinos at the Sudbury Neutrino Observatory,” *Phys. Rev. Lett.* **87**, 071301 (2001).
- [23] M. H. Ahn *et al.* [K2K Collaboration], “Indications of neutrino oscillation in a 250 km long baseline experiment,” *Phys. Rev. Lett.* **90**, 041801 (2003).
- [24] K. Eguchi *et al.* [KamLAND Collaboration], “First results from KamLAND: Evidence for reactor anti-neutrino disappearance,” *Phys. Rev. Lett.* **90**, 021802 (2003).
- [25] K. Abe *et al.* [T2K Collaboration], “Indication of Electron Neutrino Appearance from an Accelerator-produced Off-axis Muon Neutrino Beam,” *Phys. Rev. Lett.* **107**, 041801 (2011).
- [26] F. P. An *et al.* [Daya Bay Collaboration], “Observation of electron-antineutrino disappearance at Daya Bay,” *Phys. Rev. Lett.* **108**, 171803 (2012).
- [27] I. Esteban, M. C. Gonzalez-Garcia, M. Maltoni, I. Martinez-Soler and T. Schwetz, “Updated fit to three neutrino mixing: exploring the accelerator-reactor complementarity,” *JHEP* **1701**, 087 (2017).
- [28] M. G. Aartsen *et al.* [IceCube Collaboration], “Evidence for Astrophysical Muon Neutrinos from the Northern Sky with IceCube,” *Phys. Rev. Lett.* **115**, no. 8, 081102 (2015).
- [29] M. C. Gonzalez-Garcia, F. Halzen and M. Maltoni, “Physics reach of high-energy and high-statistics icecube atmospheric neutrino data,” *Phys. Rev. D* **71**, 093010 (2005).
- [30] R. Abbasi *et al.* [IceCube Collaboration], “The IceCube Data Acquisition System: Signal Capture, Digitization, and Timestamping,” *Nucl. Instrum. Meth. A* **601**, 294-316 (2009).
- [31] M. G. Aartsen *et al.* [IceCube Collaboration], “The IceCube Neutrino Observatory: Instrumentation and Online Systems,” *JINST* **12**, no. 03, P03012 (2017).
- [32] C. N. Weaver, “Evidence for Astrophysical Muon Neutrinos from the Northern Sky,” PhD thesis, University of Wisconsin, Madison (2015).
- [33] A. Fedynitch, R. Engel, T. K. Gaisser, F. Riehn and T. Stanev, “Calculation of conventional and prompt lepton fluxes at very high energy,” *EPJ Web Conf.* **99**, 08001 (2015).
- [34] B. J. P. Jones, “Sterile Neutrinos in Cold Climates,” PhD thesis, MIT (2015).
- [35] C. A. Argüelles Delgado, “New Physics with Atmospheric Neutrinos,” PhD thesis, University of Wisconsin at Madi-

- son (2015).
- [36] A. Cooper-Sarkar and S. Sarkar, “Predictions for high energy neutrino cross-sections from the ZEUS global PDF fits,” *JHEP* **0801**, 075 (2008).
- [37] M. G. Aartsen *et al.* [IceCube Collaboration], “Searches for Sterile Neutrinos with the IceCube Detector,” *Phys. Rev. Lett.* **117**, no. 7, 071801 (2016).
- [38] D. Foreman-Mackey, D. W. Hogg, D. Lang, and J. Goodman, “emcee: The MCMC Hammer,” *Publ. Astron. Soc. Pac.* **125**, 306-312 (2013).
- [39] M. G. Aartsen *et al.* [IceCube Collaboration], “Determining neutrino oscillation parameters from atmospheric muon neutrino disappearance with three years of IceCube DeepCore data,” *Phys. Rev. D* **91**, no. 7, 072004 (2015).
- [40] R. A. Harris and L. Stodolsky, “Two State Systems in Media and ‘Turing’s Paradox.’” *Phys. Lett. B* **116**, 464-468 (1982).
- [41] J. Abraham *et al.* [Pierre Auger Collaboration], “Observation of the suppression of the flux of cosmic rays above 4×10^{19} eV,” *Phys. Rev. Lett.* **101**, 061101 (2008).
- [42] A. Aab *et al.* [Pierre Auger Collaboration], “Evidence for a mixed mass composition at the ‘ankle’ in the cosmic-ray spectrum,” *Phys. Lett. B* **762**, 288-295 (2016).
- [43] Matthew Chalmers, “Interview: Steven Weinberg,” *CERN Courier*, November 2017, **57** issue 9, 31-35.
- [44] M. G. Aartsen *et al.* [IceCube Collaboration], “Evidence for High-Energy Extraterrestrial Neutrinos at the IceCube Detector,” *Science* **342**, 1242856 (2013).
- [45] F. W. Stecker, S. T. Scully, S. Liberati and D. Mattingly, “Searching for Traces of Planck-Scale Physics with High Energy Neutrinos,” *Phys. Rev. D* **91**, no. 4, 045009 (2015).
- [46] C. A. Argüelles, T. Katori and J. Salvado, “New Physics in Astrophysical Neutrino Flavor,” *Phys. Rev. Lett.* **115**, 161303 (2015).
- [47] M. G. Aartsen *et al.* [IceCube Collaboration], “Measurement of South Pole ice transparency with the IceCube LED calibration system,” *Nucl. Instrum. Meth. A* **711**, 73-89 (2013).
- [48] M. G. Aartsen *et al.* [IceCube Collaboration], “Measurement of the Atmospheric ν_e Spectrum with IceCube,” *Phys. Rev. D* **91**, 122004 (2015).
- [49] S. Adrian-Martinez *et al.* [KM3Net Collaboration], “Letter of intent for KM3NeT 2.0,” *J. Phys. G* **43**, no. 8, 084001 (2016).
- [50] M. G. Aartsen *et al.* [IceCube Collaboration], “IceCube-Gen2: A Vision for the Future of Neutrino Astronomy in Antarctica,” *PoS FRAPWS* **2016**, 004 (2017).
- [51] M. Altmann *et al.* [GNO Collaboration], “GNO solar neutrino observations: Results for GNO I,” *Phys. Lett. B* **490**, 16-26 (2000).
- [52] J. N. Abdurashitov *et al.* [SAGE Collaboration], “Solar neutrino flux measurements by the Soviet-American Gallium Experiment (SAGE) for half the 22 year solar cycle,” *J. Exp. Theor. Phys.* **95**, 181 (2002) [*Zh. Eksp. Theor. Fiz.* **122**, 211 (2002)].
- [53] J. Hosaka *et al.* [Super-Kamiokande Collaboration], “Solar neutrino measurements in super-Kamiokande-I,” *Phys. Rev. D* **73**, 112001 (2006).
- [54] B. Aharmim *et al.* [SNO Collaboration], “Electron energy spectra, fluxes, and day-night asymmetries of B-8 solar neutrinos from measurements with NaCl dissolved in the heavy-water detector at the Sudbury Neutrino Observatory,” *Phys. Rev. C* **72**, 055502 (2005).
- [55] C. Arpesella *et al.* [Borexino Collaboration], “Direct Measurement of the Be-7 Solar Neutrino Flux with 192 Days of Borexino Data,” *Phys. Rev. Lett.* **101**, 091302 (2008).
- [56] Y. Ashie *et al.* [Super-Kamiokande Collaboration], “Evidence for an oscillatory signature in atmospheric neutrino oscillation,” *Phys. Rev. Lett.* **93**, 101801 (2004).
- [57] P. Adamson *et al.* [MINOS Collaboration], “Combined analysis of ν_μ disappearance and $\nu_\mu \rightarrow \nu_e$ appearance in MINOS using accelerator and atmospheric neutrinos,” *Phys. Rev. Lett.* **112**, 191801 (2014).
- [58] M. G. Aartsen *et al.* [IceCube Collaboration], “Measurement of Atmospheric Neutrino Oscillations at 6–56 GeV with IceCube DeepCore,” *Phys. Rev. Lett.* **120**, no. 7, 071801 (2018).
- [59] S. Abe *et al.* [KamLAND Collaboration], “Precision Measurement of Neutrino Oscillation Parameters with KamLAND,” *Phys. Rev. Lett.* **100**, 221803 (2008).
- [60] Y. Abe *et al.* [Double Chooz Collaboration], “Indication of Reactor $\bar{\nu}_e$ Disappearance in the Double Chooz Experiment,” *Phys. Rev. Lett.* **108**, 131801 (2012).
- [61] J. K. Ahn *et al.* [RENO Collaboration], “Observation of Reactor Electron Antineutrino Disappearance in the RENO Experiment,” *Phys. Rev. Lett.* **108**, 191802 (2012).
- [62] F. P. An *et al.* [Daya Bay Collaboration], “Spectral measurement of electron antineutrino oscillation amplitude and frequency at Daya Bay,” *Phys. Rev. Lett.* **112**, 061801 (2014).
- [63] K. Abe *et al.* [T2K Collaboration], “Combined Analysis of Neutrino and Antineutrino Oscillations at T2K,” *Phys. Rev. Lett.* **118**, no. 15, 151801 (2017).
- [64] P. Adamson *et al.* [NOvA Collaboration], “Constraints on Oscillation Parameters from ν_e Appearance and ν_μ Disappearance in NOvA,” *Phys. Rev. Lett.* **118**, no. 23, 231801 (2017).
- [65] S. R. Coleman and S. L. Glashow, “High-energy tests of Lorentz invariance,” *Phys. Rev. D* **59**, 116008 (1999).
- [66] G. Amelino-Camelia, J. R. Ellis, N. E. Mavromatos, D. V. Nanopoulos and S. Sarkar, “Tests of quantum gravity from observations of gamma-ray bursts,” *Nature* **393**, 763-765 (1998).
- [67] D. Colladay and V. A. Kostelecky, “CPT violation and the standard model,” *Phys. Rev. D* **55**, 6760-6774 (1997).
- [68] D. Colladay and V. A. Kostelecky, “Lorentz violating extension of the standard model,” *Phys. Rev. D* **58**, 116002 (1998).
- [69] V. A. Kostelecky, “Gravity, Lorentz violation, and the standard model,” *Phys. Rev. D* **69**, 105009 (2004).
- [70] L. B. Auerbach *et al.* [LSND Collaboration], “Tests of Lorentz violation in anti- $\nu(\mu) \rightarrow \bar{\nu}_i$ anti- $\nu(e)$ oscillations,” *Phys. Rev. D* **72**, 076004 (2005).
- [71] A. A. Aguilar-Arevalo *et al.* [MiniBooNE Collaboration], “Test of Lorentz and CPT violation with Short Baseline Neutrino Oscillation Excesses,” *Phys. Lett. B* **718**, 1303-1308 (2013).
- [72] P. Adamson *et al.* [MINOS Collaboration], “Testing Lorentz Invariance and CPT Conservation with NuMI Neutrinos in the MINOS Near Detector,” *Phys. Rev. Lett.* **101**, 151601 (2008).
- [73] P. Adamson *et al.* [MINOS Collaboration], “A Search for Lorentz Invariance and CPT Violation with the MINOS Far Detector,” *Phys. Rev. Lett.* **105**, 151601 (2010).
- [74] P. Adamson *et al.* [MINOS Collaboration], “Search for

- Lorentz invariance and CPT violation with muon antineutrinos in the MINOS Near Detector,” *Phys. Rev. D* **85**, 031101 (2012).
- [75] B. Rebel and S. Mufson, “The Search for Neutrino-Antineutrino Mixing Resulting from Lorentz Invariance Violation using neutrino interactions in MINOS,” *Astropart. Phys.* **48**, 78-81 (2013).
- [76] Y. Abe *et al.* [Double Chooz Collaboration], “First Test of Lorentz Violation with a Reactor-based Antineutrino Experiment,” *Phys. Rev. D* **86**, 112009 (2012).
- [77] J. S. Díaz, T. Katori, J. Spitz and J. M. Conrad, “Search for neutrino-antineutrino oscillations with a reactor experiment,” *Phys. Lett. B* **727**, 412 (2013).
- [78] J. S. Diaz and T. Schwetz, “Limits on CPT violation from solar neutrinos,” *Phys. Rev. D* **93**, no. 9, 093004 (2016).
- [79] K. Abe *et al.*, “Search for Lorentz and CPT violation using sidereal time dependence of neutrino flavor transitions over a short baseline,” *Phys. Rev. D* **95**, no. 11, 111101 (2017).
- [80] F. Feroz, M. P. Hobson and M. Bridges, “MultiNest: an efficient and robust Bayesian inference tool for cosmology and particle physics,” *Mon. Not. Roy. Astron. Soc.* **398**, 1601-1614 (2009).

We acknowledge the support from the following agencies: USA – U.S. National Science Foundation-Office of Polar Programs, U.S. National Science Foundation-Physics Division, Wisconsin Alumni Research Foundation, Center for High Throughput Computing (CHTC) at the University of Wisconsin-Madison, Open Science Grid (OSG), Extreme Science and Engineering Discovery Environment (XSEDE), U.S. Department of Energy-National Energy Research Scientific Computing Center, Particle astrophysics research computing center at the University of Maryland, Institute for Cyber-Enabled Research at Michigan State University, and Astroparticle physics computational facility at Marquette University; Belgium – Funds for Scientific Research (FRS-FNRS and FWO), FWO Odysseus and Big Science programmes, and Belgian Federal Science Policy Office (Belspo); Germany – Bundesministerium für Bildung und Forschung (BMBF), Deutsche Forschungsgemeinschaft (DFG), Helmholtz Alliance for Astroparticle Physics (HAP), Initiative and Networking Fund of the Helmholtz Association, Deutsches Elektronen Synchrotron (DESY), and High Performance Computing cluster of the RWTH Aachen; Sweden – Swedish Research Council, Swedish Polar Research Secretariat, Swedish National Infrastructure for Computing (SNIC), and Knut and Alice Wallenberg Foundation; Australia – Australian Research Council; Canada – Natural Sciences and Engineering Research Council of Canada, Calcul Québec, Compute Ontario, Canada Foundation for Innovation, WestGrid, and Compute Canada; Denmark – Villum Fonden, Danish National Research Foundation (DNRF); New Zealand – Marsden Fund; Japan – Japan Society for Promotion of Science (JSPS), and Institute for Global Prominent Research (IGPR) of Chiba University; Korea – National Research Foundation of Korea (NRF); Switzerland – Swiss

National Science Foundation (SNSF); United Kingdom – Science and Technology Facilities Council (STFC), and The Royal Society.

Author contributions

The IceCube Collaboration designed, constructed and now operates the IceCube Neutrino Observatory. Data processing and calibration, Monte Carlo simulations of the detector and of theoretical models, and data analyses were performed by a large number of collaboration members, who also discussed and approved the scientific results presented here. The main authors of this manuscript were C. Argüelles, A. Kheirakdish, G. Collin, S. Mandalia, J. Conrad, and T. Katori. It was reviewed by the entire collaboration before publication, and all authors approved the final version of the manuscript.

Competing financial interests

The authors declare no competing financial interests.

Supplemental materials

Neutrino oscillations and tests of Lorentz violation

The field of neutrino oscillations has been developed through a series of measurements of Solar [51–55], atmospheric [56–58], reactor [59–62], and accelerator neutrinos [57, 63, 64]. In the early days, the cause of neutrino oscillations was not precisely known, and Lorentz violation was suggested as a possible source of neutrino flavour anomalies [65] and so tests of Lorentz violation with high-energy astrophysical sources started to generate a lot of interest [66]. Subsequently, the L/E dependence of standard neutrino oscillations was measured [56]. Because the neutrino mass term in the effective Hamiltonian has a $1/E$ energy dependence, it was a strong indication that a nonzero neutrino mass is in fact the cause of neutrino oscillations, not Lorentz violation. Then, the focus of the community shifted to consider Lorentz violation to be a second order effect in neutrino oscillations, and so neutrino oscillation data has been used to look for small deviations due to Lorentz violation from the standard neutrino mass oscillations.

One approach to look for LV is to use a model-independent effective field theory, such as the Standard-Model Extension (SME) [67, 68]. SME is widely accepted in communities from low-energy table top experiments to high-energy particle physics and cosmology, to search for Lorentz violation. This formalism incorporates various fundamental features of quantum field theories, such as energy-momentum conservation, observer

Lorentz transformations, and spin-statistics, however it includes violations of particle Lorentz transformations. A number of neutrino oscillation data sets have been analyzed using this formalism, including LSND [70], Mini-BooNE [71], MINOS [72–75], Double Chooz [76, 77], SNO [78], T2K [79], as well as the aforementioned IceCube-40 and Super-Kamiokande. These experiments can be classified into two groups. First, the presence of a direction-dependent field induces direction-dependent physics. In particular, neutrino beam lines are fixed and so such direction-dependent physics would show up as a time-dependence of neutrino oscillation data [70–76, 78, 79]. Second, a search of Lorentz violation is possible even without assuming the presence of a spatial component, *i.e.* no time-dependent physics, by utilizing distortions of the spectrum [77]. The results presented in this article are based on this second approach.

Neutrino oscillation formula

Here, we illustrate how to calculate the oscillation probability for the case with nonzero isotropic Lorentz violations, such as $\hat{a}^{(d)}$ and $\hat{c}^{(d)}$. The effective Hamiltonian relevant for oscillation is given by

$$H \sim \frac{m^2}{2E} + \sum_{d \geq 3} E^{d-3} (\hat{a}^{(d)} - \hat{c}^{(d)}).$$

Note that $\hat{a}^{(d)}$ are nonzero for $d = \text{odd}$, and $\hat{c}^{(d)}$ are nonzero for $d = \text{even}$. We assume that either one of them is nonzero. We use $\nu_\mu \rightarrow \nu_\tau$ two-flavour approximation which allows us to solve the time-dependent Schrödinger equation analytically to derive the neutrino oscillation formula with neutrino masses and LV. This choice is allowed because a large matter potential "arrests" ν_e (quantum Zeno effect [40]) and prevent transitions from ν_μ . Since the matter potential of ν_e is much bigger than that due to Lorentz violation effects, the size of Lorentz violation that we consider here hardly induces any $\nu_\mu \rightarrow \nu_e$ transition. Our choice of the two-flavour oscillation model does not diminish the strength of our constraints on parameters in the $\nu_\mu - \nu_\tau$ block matrix with respect to a full three flavour calculation. Hence, the mass matrix m^2 can be diagonalized to $M^2 = \text{diag}(m_2^2, m_3^2)$ by a mixing matrix U with mixing angle ϕ ,

$$\begin{aligned} m^2 &= U M^2 U^\dagger \\ &= \begin{pmatrix} \cos \phi & \sin \phi \\ -\sin \phi & \cos \phi \end{pmatrix} \begin{pmatrix} m_2^2 & 0 \\ 0 & m_3^2 \end{pmatrix} \begin{pmatrix} \cos \phi & -\sin \phi \\ \sin \phi & \cos \phi \end{pmatrix}. \end{aligned}$$

By adding $E^{d-3}(\hat{a}^{(d)} - \hat{c}^{(d)})$, this 2×2 Hamiltonian can be diagonalized with two eigenvalues, λ_1 and λ_2 . Here, we define $\lambda_2 > \lambda_1$. Then the oscillation formula is

$$P(\nu_\mu \rightarrow \nu_\tau) = \frac{|2A_2|^2}{(\lambda_2 - \lambda_1)^2} \sin^2 \left(\frac{\lambda_2 - \lambda_1}{2} L \right)$$

where

$$\begin{aligned} \lambda_1 &= \frac{1}{2} \left[(A_1 + A_3) - \sqrt{|A_1 - A_3|^2 + |2A_2|^2} \right] \\ \lambda_2 &= \frac{1}{2} \left[(A_1 + A_3) + \sqrt{|A_1 - A_3|^2 + |2A_2|^2} \right] \\ A_1 &= \frac{1}{2E} (m_2^2 \cos^2 \phi + m_3^2 \sin^2 \phi) + E^{d-3} (\hat{a}_{\mu\mu}^{(d)} - \hat{c}_{\mu\mu}^{(d)}) \\ A_2 &= \frac{1}{2E} \cos \phi \sin \phi (m_2^2 - m_3^2) + E^{d-3} (\hat{a}_{\mu\tau}^{(d)} - \hat{c}_{\mu\tau}^{(d)}) \\ A_3 &= \frac{1}{2E} (m_2^2 \sin^2 \phi + m_3^2 \cos^2 \phi) - E^{d-3} (\hat{a}_{\mu\mu}^{(d)} - \hat{c}_{\mu\mu}^{(d)}). \end{aligned}$$

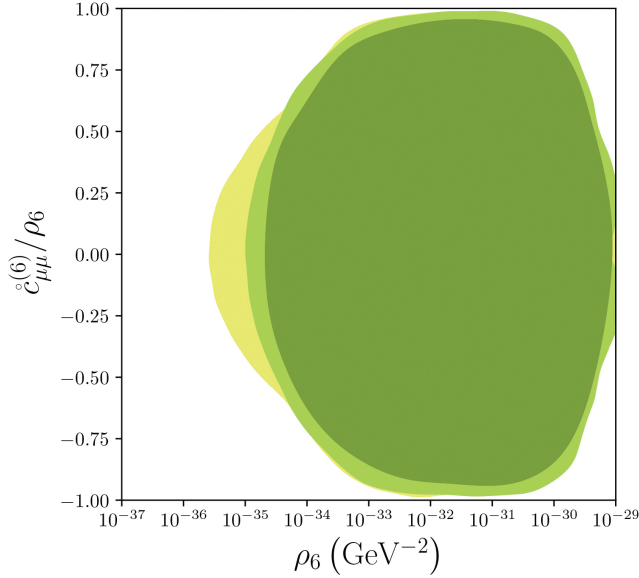
In the high-energy limit, the neutrino mass effect is negligible in comparison to Lorentz violating effects,

$$\begin{aligned} P(\nu_\mu \rightarrow \nu_\tau) &\sim \left(1 - \frac{[\hat{a}_{\mu\mu}^{(d)} - \hat{c}_{\mu\mu}^{(d)}]^2}{\rho_d^2} \right) \sin^2(L\rho_d \cdot E^{d-3}) \\ &= \frac{|\hat{a}_{\mu\tau}^{(d)} - \hat{c}_{\mu\tau}^{(d)}|^2}{\rho_d^2} \sin^2(L\rho_d \cdot E^{d-3}). \end{aligned}$$

Here we use $\rho_d \equiv \sqrt{(\hat{a}_{\mu\mu}^{(d)})^2 + \text{Re}(\hat{a}_{\mu\tau}^{(d)})^2 + \text{Im}(\hat{a}_{\mu\tau}^{(d)})^2}$ or $\sqrt{(\hat{c}_{\mu\mu}^{(d)})^2 + \text{Re}(\hat{c}_{\mu\tau}^{(d)})^2 + \text{Im}(\hat{c}_{\mu\tau}^{(d)})^2}$, which represents the strength of LV. Then, $\hat{a}_{\mu\mu}^{(d)}/\rho_d$ and $\hat{c}_{\mu\mu}^{(d)}/\rho_d$ become fractions of diagonal terms which are bounded between -1 and $+1$. The result suggests there are no LV neutrino oscillations without off-diagonal terms and that the LV oscillations are symmetric between the real and imaginary parts of the off-diagonal SME parameters.

Results using Bayesian framework

The main results of this paper are extracted using Wilks' theorem so as to be directly comparable with frequentist results reported by other neutrino experiments. For completeness, we have also performed a Bayesian analysis which uses a joint distribution over the nine systematic and LV parameters. This joint distribution is constructed from the same likelihood and prior distributions used in the frequentist analysis, except that we also added conservative constraints on all flux normalizations to avoid a strong prior range dependence. The Bayesian study is presented in two results (see in Supplementary Figure 1), which were both generated by the EMCEE Markov Chain Monte Carlo software package [38]. First, we constructed the 99% exclusion credibility region (C.R.) from a sampling of the joint distribution, with two different treatments on nuisance parameters. Second, we extracted the result based on the Bayes factor of marginalizing the likelihood over nuisance parameters using the MultiNest algorithm [80]. These studies highlight the differences in results obtained using different treatments of nuisance parameters.

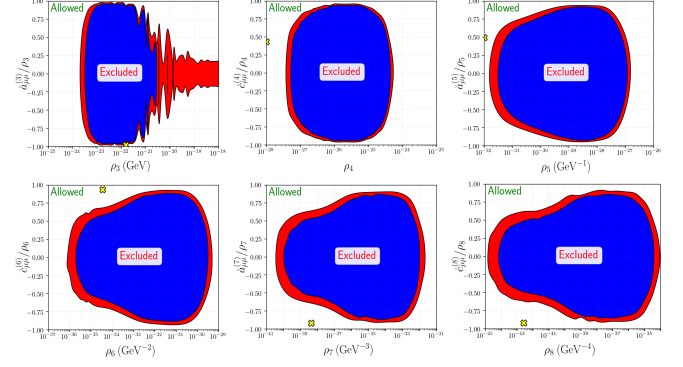


SUPPL. FIG. 1: The figure represents the posterior distribution on the dimension-six operator parameters marginalized (light green) or profiled (yellow) over all nuisance parameters. Both contours correspond to the exclusion with 99% credibility region (C.R.). The dark green area corresponds to a Bayes factor $\mathcal{B} > 10^{1.5}$ with respect to the null hypothesis.

Supplementary Figure 1 shows the example of Bayesian studies for dimension-six operators. First, we have constructed the 99% exclusion credibility region (C.R.) from a sampling of the joint distribution, which is shown (light green contour). The shape differences observed between our main frequentist result and this one arise from the different statistical treatment of nuisance parameters. In a Bayesian analysis, nuisance parameters are marginalized instead of the profiling method used in a frequentist analysis. To demonstrate this, in Suppl. Fig. 1, we also show the credibility region where nuisance parameters are profiled (yellow contour).

Second, we also report the Bayes factor (\mathcal{B}) as a function of the LV parameter space. The Bayes factor is the ratio of Bayesian evidence between the LV hypotheses and the no-LV hypothesis. In this result, the Bayesian evidence is found by marginalizing the likelihood over all parameters except for ρ_d and $\hat{c}_{\mu\mu}^{(6)}/\rho_6$. This is also shown in Supplementary Figure 1. According to Jeffreys' scale, a Bayes factor $\mathcal{B} > 10^{1.5}$ (dark green contour) is rejected with very strong strength-of-evidence. As expected, the Bayesian evidence based test has less reach with respect to the maximum likelihood ratio test used in the frequentist result, and it is consistent with the credibility region

with marginalized nuisance parameters (light green contour).

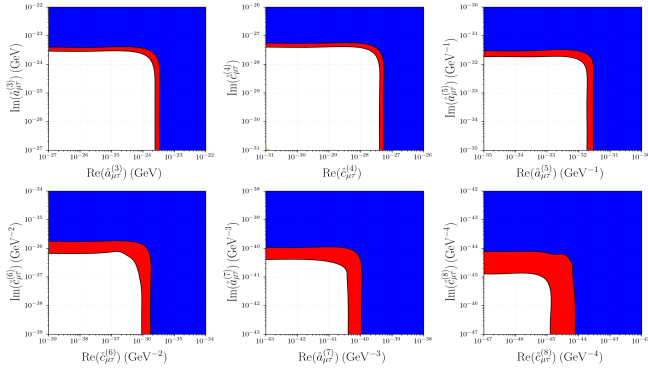


SUPPL. FIG. 2: These plots show the excluded parameter space with full parameter correlations. The x-axis represents the strength of the LV, and the y-axis shows the particular combination of SME coefficients. The dimension of the operator d increases from 3 to 8 in these plots, from left to right, and top to bottom. The red (blue) regions are excluded at 90% (99%) C.L. as we discussed, near $\cos\theta_d = -1$ and $+1$, and at large values of $\rho^{(d)}$. The best-fit points are shown by the yellow crosses.

Full fit results from Wilks' theorem

Supplementary Figure 2 shows the full-fit results from a two-flavour $\mu-\tau$ oscillation hypothesis with dimension-three to -eight LV operators. The x-axis represents the strength of LV, $\rho_d \equiv \sqrt{(\hat{a}_{\mu\mu}^{(d)})^2 + \text{Re}(\hat{a}_{\mu\tau}^{(d)})^2 + \text{Im}(\hat{a}_{\mu\tau}^{(d)})^2}$ or $\sqrt{(\hat{c}_{\mu\mu}^{(d)})^2 + \text{Re}(\hat{c}_{\mu\tau}^{(d)})^2 + \text{Im}(\hat{c}_{\mu\tau}^{(d)})^2}$, and the y-axis represents a fraction of the diagonal element, $\hat{a}_{\mu\mu}^{(d)}/\rho_d$ or $\hat{c}_{\mu\mu}^{(d)}/\rho_d$. The best-fit values indicate no LV, and we draw exclusion curves for 90% C.L. (red) and 99% C.L. (blue). The best fit points are shown with markers. If the best fit points are outside the plotting region, markers are set at the edge. The overlap of contours from different dimension operators indicate that it is possible that two operators from different dimensions show up in the same energy scale.

Low dimension operators may be accessible by existing atmospheric neutrino oscillation experiments. For example, the DeepCore oscillation analysis utilizes 10 – 100 GeV atmospheric neutrinos with a baseline equal to the Earth's diameter. This implies that the experiment has sensitivity to LV both via spectrum distortions and normalization changes of the flux, up to roughly a 10^{-23} GeV limit on $\hat{a}^{(3)}$ or ρ_3 .



SUPL. FIG. 3: These plots show limits on off-diagonal parameters in the case when diagonal parameters are set to zero. The dimension of the operator d increases from 3 to 8 in these plots, from left to right, and top to bottom. The red (blue) regions are excluded at 90% (99%) C.L. There are four identical plots depending on the sign of the real and imaginary parts, but here we only show the cases when both the real and imaginary parts are positive.